

# **Study of a Naturally Oscillating Triangular-Jet Flow**

by

**Soon-Kong Lee**

THE UNIVERSITY OF ADELAIDE  
School of Mechanical Engineering  
South Australia, 5005, AUSTRALIA

for

**the Degree of Doctor of Philosophy**

Copyright © February 2009, S. K. Lee

# Contents

<b>Abstract</b>	<b>vii</b>
<b>Acknowledgements</b>	<b>xi</b>
<b>Declaration</b>	<b>xii</b>
<b>List of figures</b>	<b>xiii</b>
<b>List of tables</b>	<b>xix</b>
<b>Notation</b>	<b>xxi</b>
<hr/>	
<b>1 Introduction</b>	<b>1</b>
1.1 Oscillating-jet flows . . . . .	1
1.2 Enhanced mixing burners . . . . .	5
1.2.1 Initial motivation . . . . .	5
1.2.2 The use of swirling-jet flows . . . . .	6
1.2.3 Origin of the “fluidic” orifice-cavity-orifice nozzle . . . . .	8
1.3 Motivation for the current project . . . . .	9
1.3.1 The fluidic-precressing-jet (FPJ) burner for mineral processing . . . . .	9
1.3.2 Cement clinker production . . . . .	11
1.3.3 Advantages of the FPJ burner . . . . .	11
1.4 Development of the Gyro-Therm burner . . . . .	13
1.4.1 Intermittency of precession . . . . .	13
1.4.2 Effect of internal “centre-body” . . . . .	14
1.4.3 Control of flame shape with a secondary flow . . . . .	16
1.4.4 Pressure loss . . . . .	16
1.4.5 Effect of inlet-orifice shape . . . . .	17
1.5 Objectives . . . . .	18
<b>2 Literature review</b>	<b>19</b>
2.1 FPJ external flow . . . . .	19
2.1.1 Initial research . . . . .	19

2.1.2	Overview of FPJ research programme . . . . .	20
2.1.3	A comparison between FPJ and axisymmetric turbulent-jet flows . . . . .	21
2.1.4	Structure of unconfined buoyant (FPJ) flames . . . . .	23
2.2	FPJ internal flow . . . . .	25
2.2.1	A qualitative model . . . . .	25
2.2.2	A proposed mechanism for jet precession . . . . .	28
2.3	Surface streaklines of deflected-jet flow in the FPJ nozzle . . . . .	31
2.3.1	Nathan's short-cavity nozzle with an external centre-body . . . . .	31
2.3.2	Hill's FPJ nozzle with a tilted inlet pipe . . . . .	31
2.3.3	Vidakovic's convergent-divergent nozzle . . . . .	35
2.4	"Backward-facing-step" flow . . . . .	37
2.4.1	Effect of step height or expansion ratio . . . . .	37
2.4.2	Separated flow region of two-dimensional backward-facing step . . . . .	37
2.5	Triangular-jet flow field . . . . .	40
2.5.1	"Dump-combustor" flows . . . . .	40
2.5.2	"Axis-switching" . . . . .	42
<b>3</b>	<b>Experimental apparatus</b>	<b>45</b>
3.1	Oscillating-jet nozzle . . . . .	45
3.2	Air-flow apparatus . . . . .	47
3.3	Water-flow apparatus . . . . .	48
3.4	Inlet-flow condition . . . . .	48
3.4.1	Technique and measurements . . . . .	49
3.4.2	Interpretation of data . . . . .	49
<b>4</b>	<b>Parametric study of the shape of the oscillating-triangular-jet (OTJ) nozzle</b>	<b>51</b>
4.1	Jet-spreading angle . . . . .	52
4.1.1	Flow visualisation of oscillating jets in air . . . . .	52
4.1.2	Flow visualisation of oscillating jets in water . . . . .	56
4.1.3	Effect of exit-lip diameter . . . . .	59
4.2	Azimuthal direction of the OTJ flow . . . . .	60
4.2.1	Streamer flow visualisation: technique and measurements . . . . .	60
4.2.2	Streamer flow visualisation: interpretation of results . . . . .	62
4.3	Flow-speed decay rate . . . . .	62
4.3.1	Nozzle-centreline flow speed of unconfined turbulent-jet flows . . . . .	63
4.3.2	Nozzle-centreline flow speed of the OTJ flows . . . . .	64
4.4	Flame visualisation . . . . .	67

4.4.1	Burner apparatus . . . . .	67
4.4.2	Experimental procedure and results . . . . .	67
4.4.3	Rendering of instantaneous flame patterns . . . . .	71
4.4.4	Celerity of the OTJ and FPJ flame puffs . . . . .	71
4.4.5	Global residence time of the OTJ and FPJ flames . . . . .	72
4.4.6	Puffing rate of the OTJ and FPJ flames . . . . .	72
4.5	Pressure/kinetic-energy loss of the nozzle . . . . .	75
4.5.1	Wall pressure upstream from nozzle inlet: experimental results . . . . .	75
4.5.2	Engineering formula for pressure loss . . . . .	76
4.5.3	Effect of Reynolds number . . . . .	77
4.5.4	Effect of inlet-orifice contraction . . . . .	78
4.5.5	Effect of exit-lip diameter . . . . .	79
4.5.6	Effect of chamber length and inlet-orifice expansion . . . . .	80
4.5.7	Optimising the pressure-loss model . . . . .	81
4.6	Summary . . . . .	82
4.6.1	Effect of chamber length and inlet-orifice expansion ratio . . . . .	82
4.6.2	Effect of exit-lip size . . . . .	83
4.6.3	Flow inside the nozzle . . . . .	83
4.6.4	Preferred azimuthal direction of the OTJ flow . . . . .	83
4.6.5	Open-flame tests . . . . .	84
4.6.6	Pressure loss of the nozzle . . . . .	84
<b>5</b>	<b>Stationary deflected triangular jet (SDTJ)</b>	<b>85</b>
5.1	Pressure contours at the nozzle-exit plane . . . . .	86
5.1.1	Experimental method . . . . .	86
5.1.2	Flow entrainment . . . . .	87
5.2	Oscillating and precessing jets . . . . .	89
5.2.1	Surface-paste technique . . . . .	89
5.2.2	Surface streaklines inside the cylindrical chamber . . . . .	89
5.2.3	Flow pattern near the exit lip . . . . .	92
5.2.4	Effect of expansion ratio on surface streaklines . . . . .	92
5.3	Undeflected and stationary-deflected (SDTJ) flow . . . . .	94
5.3.1	Wall-pressure distribution: technique and measurements . . . . .	94
5.3.2	Interpretation of SDTJ surface-pressure and flow-visualisation images . . . . .	95
5.4	Visualisation of SDTJ flow using air bubbles . . . . .	98
5.4.1	Experimental method . . . . .	98

5.4.2	Observations . . . . .	98
5.5	Model of SDTJ flow reattachment . . . . .	101
5.5.1	Vortex skeleton . . . . .	101
5.5.2	Assembling the flow model . . . . .	101
5.6	Effect of changing the inlet-boundary condition . . . . .	103
5.7	Summary . . . . .	104
<b>6</b>	<b>Structure of oscillating-triangular-jet (OTJ) flow: pressure measurements</b>	<b>105</b>
6.1	Event detection: azimuthal orientation of deflected jet . . . . .	106
6.1.1	Equipment layout and description of pressure transducer . . . . .	106
6.1.2	Direct observation of events . . . . .	108
6.1.3	Instrumentation: filter and comparator . . . . .	108
6.1.4	Validation of event detection: comparator output . . . . .	110
6.1.5	Detection of non-oscillating flow states in the OTJ nozzle . . . . .	110
6.1.6	Switching between undeflected and stationary-deflected (SDTJ) flow . . . . .	113
6.2	Event detection: direction of jet oscillation . . . . .	115
6.2.1	Location of (additional) pressure probes . . . . .	115
6.2.2	Direction-detection algorithm . . . . .	116
6.2.3	Validation of direction-detection algorithm . . . . .	116
6.3	Wall-pressure distribution in the OTJ nozzle . . . . .	119
6.3.1	Conditionally-averaged wall pressure . . . . .	120
6.3.2	Theoretical basis of the modified Phillips method . . . . .	120
6.3.3	Modified Phillips estimate of wall pressure . . . . .	122
6.3.4	Reconstruction of the OTJ surface-flow pattern . . . . .	124
6.3.5	Pressure force on the deflected-jet flow . . . . .	126
6.3.6	Estimate of jet deflection . . . . .	128
6.4	Strouhal number of oscillation . . . . .	130
6.4.1	Experimental method . . . . .	131
6.4.2	Strouhal number of the precessing jet: review of measurements . . . . .	133
6.4.3	Oscillation rate of the orifice-plate FPJ flow . . . . .	135
6.4.4	Oscillation rate of the smooth-contraction “long-cavity” flow . . . . .	137
6.4.5	Observed oscillation rate of the OTJ flow . . . . .	137
6.5	Summary . . . . .	138
6.5.1	Pressure probe for event detection . . . . .	138
6.5.2	Switching between flow states . . . . .	138
6.5.3	Method of direction detection . . . . .	139

6.5.4	Conditionally-averaged wall-pressure distribution of the OTJ flow . . .	139
6.5.5	Strouhal number of the oscillating/precessing jet . . . . .	140
<b>7</b>	<b>Conditional particle image velocimetry (PIV): experimental technique</b>	<b>141</b>
7.1	Basic principles of PIV . . . . .	142
7.2	PIV apparatus . . . . .	144
7.2.1	Pulse laser . . . . .	144
7.2.2	Optics . . . . .	146
7.2.3	Digital photography . . . . .	146
7.2.4	Seeding . . . . .	146
7.3	PIV timing . . . . .	147
7.3.1	Settings of the laser and the camera . . . . .	147
7.3.2	Proximity of laser-light sheet and the inlet orifice . . . . .	149
7.4	Conditional sampling . . . . .	150
7.5	Method of processing velocity data . . . . .	151
7.5.1	Velocity resolution . . . . .	156
7.5.2	Spatial resolution . . . . .	158
7.5.3	Streamlines . . . . .	158
7.6	Accuracy of velocity measurements . . . . .	160
7.6.1	Bias uncertainty in experimental technique . . . . .	160
7.6.2	Uncertainty due to unsteadiness of the flow . . . . .	162
7.7	Method of processing vorticity data . . . . .	163
7.8	Accuracy of vorticity measurements . . . . .	166
7.8.1	Bias error in vorticity calculations . . . . .	166
7.8.2	Propagation uncertainty in vorticity calculations . . . . .	172
<b>8</b>	<b>Structure of oscillating-triangular-jet (OTJ) flow: conditionally-sampled velocity</b>	<b>173</b>
8.1	Experimental method . . . . .	173
8.2	Conditional mean and r.m.s. velocity fields . . . . .	174
8.3	Streamlines . . . . .	180
8.3.1	Reliability of flow patterns . . . . .	182
8.3.2	Stationary deflected triangular jet (SDTJ) . . . . .	185
8.3.3	Oscillating triangular jet (OTJ) . . . . .	186
8.4	Vorticity . . . . .	189
8.4.1	Internal flow . . . . .	194
8.4.2	External flow . . . . .	194
8.5	Vortex skeleton of the ensemble-averaged flow . . . . .	195

8.5.1	SDTJ vortex skeleton . . . . .	195
8.5.2	OTJ vortex skeleton . . . . .	196
8.5.3	Circulation . . . . .	197
8.5.4	Difference between SDTJ and OTJ flows . . . . .	201
8.5.5	Corner eddy near the backward-facing step . . . . .	201
8.5.6	“Closed-surface-flow” topology . . . . .	201
8.6	Comparison of OTJ model with earlier observations . . . . .	204
8.6.1	Sink vortex on the chamber wall: numerical simulation . . . . .	204
8.6.2	Swirling flow at the inlet end of the chamber . . . . .	205
8.6.3	Side-view recirculation and reverse flow . . . . .	206
8.6.4	Effect of centre-body . . . . .	206
8.7	Summary . . . . .	208
8.7.1	Ensemble-averaged velocity fields: mean and r.m.s. distributions . . . . .	208
8.7.2	Streamlines of chamber cross-section . . . . .	209
8.7.3	Distribution of streamwise vorticity . . . . .	209
8.7.4	Vortex skeleton of the non-oscillating and oscillating deflected flows . . . . .	209
<b>9</b>	<b>Conclusions</b>	<b>211</b>
9.1	Observations from flow visualisation . . . . .	212
9.2	Pressure loss in the nozzle . . . . .	212
9.3	Structure of the stationary-deflected (SDTJ) flow . . . . .	213
9.4	Surface structure of the oscillating (OTJ) flow . . . . .	214
9.5	Ensemble-averaged vortex structure . . . . .	215
	<b>References</b>	<b>217</b>
<hr/>		
	<b>Appendices</b>	<b>227</b>
<b>A</b>	<b>Nozzle-discharge coefficient</b>	<b>227</b>
<b>B</b>	<b>Direction detector: additional notes</b>	<b>229</b>
<b>C</b>	<b>Estimating jet deflection from wall-pressure distribution</b>	<b>231</b>
<b>D</b>	<b>Conditionally-sampled velocity fields</b>	<b>237</b>
<b>E</b>	<b>Associated publications</b>	<b>253</b>

# Abstract

This thesis reports on the structure of the flow inside a nozzle which produces a naturally oscillating jet flow. The nozzle consists of a short cylindrical chamber with a concentric triangular-inlet orifice at one end and a circular exit lip at the other end. This triangular-jet nozzle was developed from the “fluidic-precessing-jet” (FPJ) nozzle, which has a similar arrangement of components, but has a circular rather than a triangular inlet. For reliably oscillating flow, the FPJ nozzle should have an inlet-to-chamber expansion ratio of at least 5.0, a chamber length-to-diameter ratio between 2.6 and 2.8, and an exit-lip height of about 0.1 chamber diameters.

The triangular-jet nozzle produces a continuously and aperiodically oscillating jet flow which is different from the FPJ flow. The oscillation occurs at smaller inlet-to-chamber expansion ratios ( $2.1 \lesssim D/d_{e1} \lesssim 3.5$ ) and over a wider range of chamber lengths ( $2.0 \lesssim L/D \lesssim 2.5$ ). The initial spreading angle of the jet flow is smaller, but is still much larger than that of non-oscillating, axisymmetric turbulent-jet flows. In addition, the external “oscillating-triangular-jet” (OTJ) flow has preferred azimuthal directions which are aligned with the three corners of the orifice. The kinetic-energy-loss coefficient of the OTJ nozzle is much smaller than that of the FPJ nozzle because oscillation occurs at much smaller inlet-to-chamber expansion ratios.

For a narrow range of length-to-diameter ratios ( $1.00 \lesssim L/D \lesssim 1.25$ ), the triangular-inlet nozzle can also produce a non-oscillating or “stationary deflected triangular jet” (SDTJ) which reattaches asymmetrically to the inside surface of the cylindrical chamber. The SDTJ has a weak tendency to oscillate, which suggests that flow patterns required for self-excited oscillation are already present in the SDTJ flow. Surface-flow visualisation and surface-pressure measurements in the SDTJ nozzle have provided the location of critical points and bifurcation lines on the chamber wall, and from this the topology of the SDTJ flow is deduced. Some details of the flow such as a jet-reattachment node near the chamber exit and a strong swirl adjacent to the inlet orifice are known from previous studies of the FPJ flow, but there are many newly observed features. The most easily identified of these are two sink-focus separation points, one on each side of the reattachment node but closer to the inlet plane. The foci counter rotate and are of unequal size. Reverse flow through the exit plane of the chamber is attracted to the larger focus.

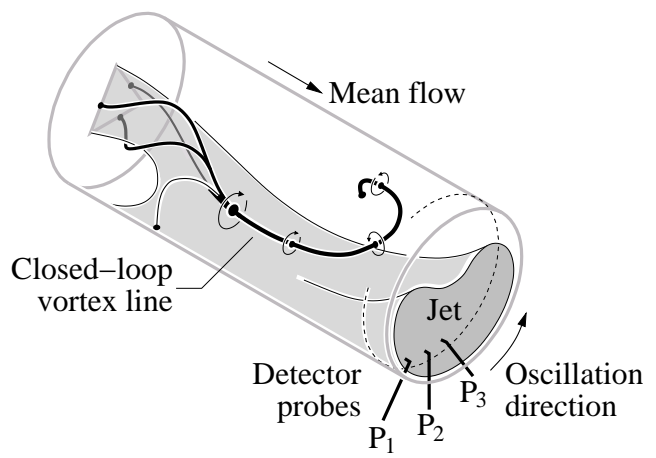
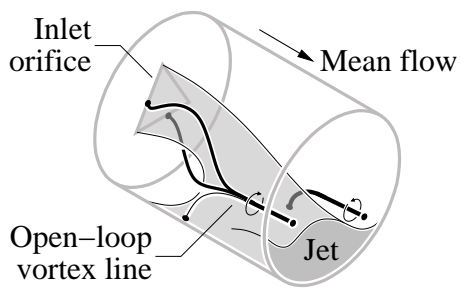
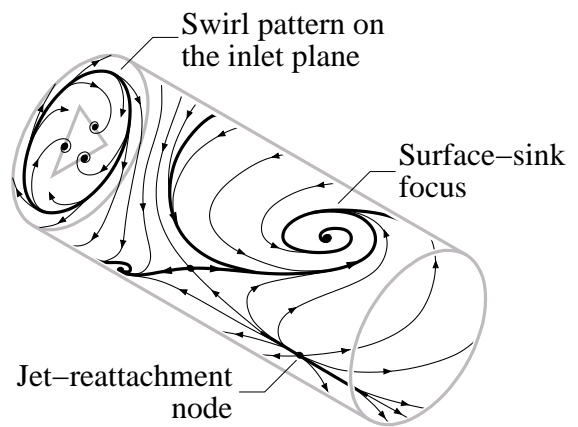
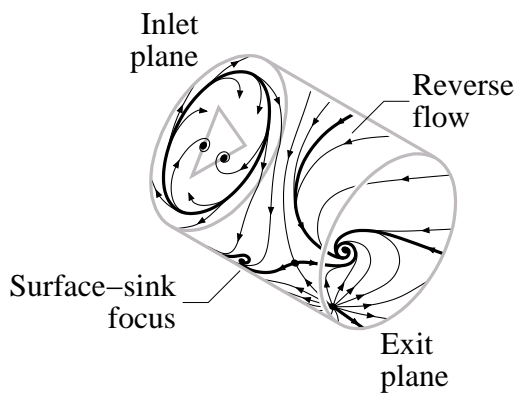
The vortex core rising from each focus is entrained by the reattaching-jet (SDTJ) flow and is drawn out of the chamber.

A backward-facing pressure probe placed in the OTJ “reattaching-flow” region of chamber wall can be used as a reliable detector of jet-flow oscillation. Cross-correlating the signal from this detector probe with simultaneous static-pressure measurements elsewhere on the chamber wall gives a conditionally-averaged pressure on the wall of the OTJ chamber. The OTJ wall-pressure distribution has the same features as the SDTJ surface-pressure distribution, but it has greater asymmetry about a mirror plane drawn through the chamber axis and the detector probe.

An array of three backward-facing pressure probes has been used as an “event detector” for conditionally-sampled (PIV) measurements of non-axial velocity components in cross-sections of the OTJ nozzle. The event-detection scheme responds only to a preselected (counter-clock-wise) direction of motion of the oscillating-jet flow. The streamline patterns constructed from the conditionally-sampled measurements confirm the presence of the jet-reattachment node, the swirl and the sink foci identified from the SDTJ surface-flow visualisation.

The shear-layer interaction between the jet from the triangular orifice and the swirl (adjacent to the inlet plane) produces strong longitudinal vortices in the ensemble-averaged flow. The jet flow distributes these vortices through the length of the chamber. Vortex cores representing the vortices are reconstructed by tracking streamline foci from one PIV cross-section plane to another. The tracking process includes the connection and termination of vortex cores in a manner which is consistent with the Helmholtz vortex law. In this flow field, the vortex core produced by the swirl and the vortex core rising from the larger sink-focus vortex on the chamber wall are connected to form a loop. The extent to which this vortex loop is contained within the chamber determines whether or not the flow is oscillating.

If only a small fraction (e.g. 8%) of the vortex circulation passes through the exit plane of the nozzle, the loop is trapped inside the chamber and the deflected jet oscillates. If the length of the chamber is halved, about 35% of vortex circulation escapes from the nozzle and the oscillation stops.



The stationary deflected triangular jet (SDTJ)

The oscillating triangular jet (OTJ)



# Acknowledgements

My gratitude and sincere thanks especially to

Prof. G. J. Nathan for securing financial aid from the ARC and FCT Combustion Pty. Ltd. in the form of an APA(I) and a Departmental Scholarship,

Prof. J. Mi for the idea of an oscillating-jet flow from a triangular orifice,

A/Prof. R. M. Kelso for his 14AFMC paper which motivated me to investigate the flow inside the oscillating-triangular-jet nozzle,

Dr. P. V. Lanspeary for his technical support and editorial assistance,

Dr. P. A. M. Kalt for teaching me PIV in the laboratory,

Mr. S. J. Hill for discussing his work on oscillating-jet flows,

Mr. R. Jager and the mechanical engineering workshop staff for manufacturing and installing the flow apparatus for my experiments,

Mr. B. Constantine for providing computer hardware and network support,

Mr. G. Osborne for preparing pressure probes necessary for measurements,

Mr. D. Franklin for supplying laboratory equipment and software for data acquisition,

Mr. S. De Ieso for advice on electronics of a detector for sensing direction of an oscillating flow,

My father C. F. Lee and mother M. Y. Hew for their constant love and care,

My sister S. C. Lee for the festivities of life, and

My grandmothers Y. K. Koo and Y. M. Chong, relatives, friends and colleagues for their joyful company, moral support, humour and good wishes.

*S. K. L.*

# Declaration

This work contains no material which has been accepted for the award of any other degree or diploma in any university or other tertiary institution and, to the best of my knowledge and belief, contains no material previously published or written by another person, except where due reference has been made in the text.

I give consent to this copy of my thesis, after accepted for the award of the degree and deposited in the University Library, being made available for loan and photocopying, subject to the provisions of the Copyright Act 1968.

*S. K. L.*  
*February, 2009*

# List of Figures

1.1	Methods of generating oscillating-jet flows. . . . .	2
1.2	Forced oscillation of jet flow [Reynolds et al., 2003]. . . . .	4
1.3	Swirling jets [Claypole and Syred, 1982]. . . . .	7
1.4	Shape and geometric parameters required for acoustic or fluidic oscillation. . . . .	8
1.5	Schematic diagram of the fluidic-precessing-jet (FPJ) flow field [Nathan, 1988]. . . . .	8
1.6	Schlieren photographs of FPJ flames and steady turbulent-jet flames. . . . .	9
1.7	Schematic diagram of a rotary cement kiln. . . . .	10
1.8	A comparison between FPJ flames and multi-jet flames in gas-fired kilns. . . . .	12
1.9	A comparison between FPJ flames and swirling-jet flames in a rotary kiln. . . . .	12
1.10	Air-bubble flow visualisation of FPJ flow and axisymmetric-jet flow. . . . .	13
1.11	Probability of FPJ precession [Hill, 1992]. . . . .	13
1.12	Photographs of FPJ flames and axisymmetric-jet flames. . . . .	14
1.13	Methods of controlling the FPJ flame. . . . .	15
1.14	Arrangement of FPJ nozzle for solid-fuel combustion [Nathan and Hill, 2002]. . . . .	17
2.1	A comparison between “snapshot” of FPJ and axisymmetric-jet flow field. . . . .	22
2.2	Nozzle-centreline mean concentration of FPJ and axisymmetric-jet flows. . . . .	22
2.3	Video-image sequences of FPJ flames [Newbold et al., 1997]. . . . .	23
2.4	FPJ flame celerity and global residence time [Newbold et al., 1997]. . . . .	23
2.5	Flame-puffing Strouhal number as a function of flame-base Froude number. . . . .	24
2.6	Nathan’s [1988] model of the flow field in the FPJ nozzle. . . . .	25
2.7	The China-clay method of surface-flow visualisation in the FPJ nozzle. . . . .	25
2.8	Surface-flow visualisation pattern in the FPJ nozzle and streakline interpretation. . . . .	26
2.9	Flow recirculation just upstream from the exit plane of the FPJ nozzle. . . . .	28
2.10	Kelso’s [2001] interpretation of the flow field in the FPJ nozzle. . . . .	29
2.11	The Kelso [2001] model of instantaneous surface streaklines in the FPJ nozzle. . . . .	30
2.12	Surface streaklines in a short-cavity FPJ nozzle with an external centre-body. . . . .	32
2.13	Hill’s [2003] FPJ surface streaklines; inlet pipe tilted $8^\circ$ from chamber axis. . . . .	33

2.14	Hill's [2003] FPJ surface streaklines; inlet pipe tilted $20^\circ$ from chamber axis. . .	34
2.15	The Vidakovic [1995] model of a stationary and symmetrically deflected jet. . .	36
2.16	Review of surface-flow topology of stationary deflected jets. . . . .	37
2.17	Two-dimensional, double-sided backward-facing-step flow. . . . .	38
2.18	Streamlines of reattaching flow downstream of a backward-facing step. . . . .	39
2.19	Comparing surface streaklines of backward-facing-step flow and FPJ flow. . . .	39
2.20	Schematic diagram of a dump-combustor flow field [Drewry, 1978]. . . . .	40
2.21	Flow visualisation of a forced triangular-jet flow with and without confinement.	41
2.22	Self-induced motion of a triangular vortex loop. . . . .	43
2.23	Streamwise-velocity contours of a turbulent triangular-jet flow [Quinn, 1990]. .	44
2.24	Centreline velocity of turbulent jets from triangular and circular orifices. . . . .	44
3.1	The oscillating-triangular-jet (OTJ) nozzle. . . . .	46
3.2	The air-flow apparatus. . . . .	46
3.3	The water-flow apparatus. . . . .	47
3.4	Radial distributions of velocity just upstream from the inlet orifice. . . . .	49
3.5	Wall scaling of velocity distribution just upstream from the open end of the pipe.	50
4.1	Silk-ribbon-streamer technique for visualisation of air-jet flow. . . . .	52
4.2	Results from streamer flow visualisation for OTJ and FPJ nozzles. . . . .	53
4.3	Enlargement of selected images from Figure 4.2. . . . .	54
4.4	Largest visible spreading angle of a streamer measured from images in Figure 4.2.	54
4.5	Air-bubble technique for visualisation of water-jet flow. . . . .	56
4.6	Air-bubble flow-visualisation images for OTJ nozzles. . . . .	57
4.7	Comparison between jet-spreading angle in air and in water for OTJ nozzles. .	58
4.8	Air-bubble visualisation and interpretation of flow field in the OTJ nozzle. . . .	58
4.9	Effect of exit-lip diameter on OTJ and FPJ spreading angles. . . . .	59
4.10	The effect of exit-lip diameter on the structure of flow through the nozzle. . . .	60
4.11	Oscillation of a streamer anchored at the centre of the OTJ nozzle-exit plane. .	61
4.12	Azimuthal orientation of the external jet flow for OTJ nozzle with a lip. . . . .	61
4.13	Azimuthal orientation of the external jet flow for OTJ nozzle without a lip. . . .	62
4.14	Centreline flow speed of turbulent jets from triangular and circular orifices. . .	63
4.15	Decay of centreline flow speed for the OTJ flows. . . . .	65
4.16	Mean slope of centreline flow-speed decay for the OTJ flows. . . . .	65
4.17	Chamber length required for max. jet-spreading angle and flow-speed decay rate.	66
4.18	Design chart for OTJ nozzle. . . . .	66
4.19	The burner apparatus. . . . .	68

4.20	Radial distributions of velocity just upstream from the burner inlet orifice. . . .	68
4.21	Long-exposure photographs of OTJ and FPJ flames (45 kW). . . . .	69
4.22	Long-exposure photographs of triangular-jet and circular-jet flames (45 kW). . .	70
4.23	Video-image sequences of OTJ, FPJ and triangular-jet flames (45 kW). . . . .	72
4.24	Quasi three-dimensional plot of the time series from Figure 4.23. . . . .	73
4.25	OTJ and FPJ flame celerity, global residence time and puffing Strouhal number.	74
4.26	Loss coefficient for triangular and circular orifices with and without a chamber.	76
4.27	Loss coefficient as a function of chamber length. . . . .	77
4.28	Discharge coefficient for triangular and circular orifices. . . . .	78
4.29	Loss coefficient of the exit lip at maximum jet-spreading angle of the OTJ flow.	79
4.30	Pressure loss based on flow speed at the vena contracta. . . . .	81
4.31	Comparison between loss-coefficient model and experimental data. . . . .	82
5.1	Pitot-pressure contours at the chamber-exit plane, showing a bi-stable flow. . .	86
5.2	Streamer visualisation and Pitot-probe measurements of a bi-stable flow. . . .	87
5.3	Radial distribution of flow speed at the nozzle-exit plane for undeflected jet. . .	88
5.4	OTJ surface-flow visualisation image and streakline interpretation. . . . .	90
5.5	FPJ surface-flow visualisation image and streakline interpretation. . . . .	91
5.6	Exit-lip detail for the FPJ and OTJ nozzles. . . . .	92
5.7	Time-averaged jet reattachment and negative bifurcation on the chamber wall. .	93
5.8	Ripple in the negative-bifurcation line on the chamber wall. . . . .	93
5.9	Surface flow of the undeflected triangular jet. . . . .	95
5.10	Surface-flow visualisation of the stationary deflected triangular jet (SDTJ). . . .	96
5.11	SDTJ flow topology on the inlet plane and on the azimuthal plane in the nozzle.	97
5.12	Visualisation of the SDTJ flow in the nozzle using air bubbles. . . . .	99
5.13	Air-bubble flow visualisation of SDTJ flow at the inlet plane. . . . .	100
5.14	Air-bubble flow visualisation of SDTJ flow at the exit plane. . . . .	100
5.15	Vortex skeleton of the SDTJ flow inferred from Figures 5.10 to 5.12 and 5.14. .	100
5.16	Closed-flow topology of SDTJ flow. . . . .	102
5.17	Topological rules for SDTJ flow. . . . .	102
5.18	Schematic surface-flow topology of stationary deflected jets. . . . .	103
6.1	The FPJ nozzle; summary of early flow-visualisation results. . . . .	105
6.2	Equipment for flow visualisation and pressure measurements in the OTJ flow. .	107
6.3	Event-detection pressure probe inside the OTJ nozzle. . . . .	107
6.4	Probe signals from the OTJ flow showing the effects of filter cut-off frequency.	109
6.5	Effect of cut-off frequency on correlation between probe signal and observations.	109

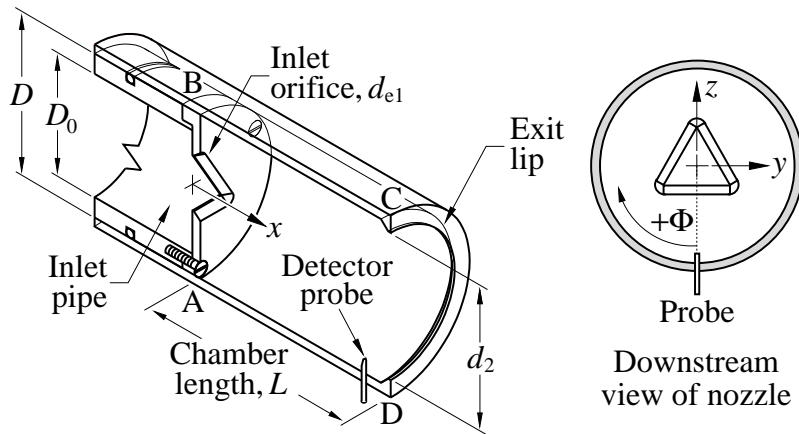
6.6	Probe signal in OTJ flows, with missed detections and spurious detections. . . .	111
6.7	Comparison of detector signals from the OTJ flows and from the FPJ flow. . . .	112
6.8	Near-surface axial-flow distribution just upstream of the SDTJ nozzle-exit plane.	113
6.9	Detector-probe signals in a bi-stable triangular-jet flow. . . . .	114
6.10	Air-bubble visualisation and 3-probe pressure measurements of the OTJ flow. .	115
6.11	Cross-correlation of two detector-probe signals in the OTJ flow. . . . .	116
6.12	The direction-detector circuit [Lanspeary and Lee, 2004]. . . . .	117
6.13	Direction-detector waveforms for counter-clockwise and clockwise oscillation.	117
6.14	Validation of direction-detector algorithm by simulation. . . . .	118
6.15	Experimental validation of direction-detector circuit. . . . .	119
6.16	Conditionally-averaged OTJ wall pressure. . . . .	121
6.17	Modified Phillips estimate of the OTJ wall pressure. . . . .	123
6.18	Interpretation of the modified Phillips estimate of the OTJ wall pressure. . . .	125
6.19	Definitions for calculating non-axial force acting on the jet flow in the chamber.	126
6.20	Non-dimensional force gradient applied to the OTJ flow and the SDTJ flow. . .	127
6.21	Deflected path of the OTJ flow and the SDTJ flow. . . . .	129
6.22	Arrangement of apparatus for measurement of oscillation rate. . . . .	131
6.23	Rate of missed/spurious detections as function of cut-off frequency. . . . .	132
6.24	Selection chart for optimum cut-off frequency of OTJ/FPJ event-detector signal.	132
6.25	Review of FPJ Strouhal-number data. . . . .	134
6.26	Strouhal number of OTJ and FPJ oscillation. . . . .	135
6.27	Jet-oscillation rate as function of expansion ratio and Reynolds number. . . . .	136
6.28	Jet-oscillation rate as function of expansion ratio only. . . . .	136
6.29	Streaklines produced by a precessing-jet flow in a long pipe [Hill et al., 1995]. .	137
7.1	Schematic diagram of double-frame two-dimensional PIV. . . . .	143
7.2	Schematic diagram of numerical method for cross-correlation PIV. . . . .	143
7.3	Arrangement of equipment for conditionally-sampled PIV in a water tank. . . .	145
7.4	Seeding particles for PIV. . . . .	147
7.5	PIV timing. . . . .	148
7.6	Effect of timing and light-sheet thickness on PIV images of the OTJ flow. . . .	149
7.7	Installation of event detector for conditionally-sampled PIV. . . . .	151
7.8	SDTJ mean and r.m.s. contours at $x/D=0.125$ . . . . .	152
7.9	SDTJ mean and r.m.s. contours at $x/D=1.375$ . . . . .	153
7.10	OTJ mean and r.m.s. contours at $x/D=0.125$ . . . . .	154
7.11	OTJ mean and r.m.s. contours at $x/D=2.625$ . . . . .	155
7.12	Uncertainty in particle displacement [Willert and Gharib, 1991]. . . . .	156

7.13	Streamlines in ensemble-averaged cross-sections of the SDTJ flow. . . . .	159
7.14	Streamlines in ensemble-averaged cross-sections of the OTJ flow. . . . .	159
7.15	Method of estimating vorticity. . . . .	163
7.16	SDTJ vorticity contours at $x/D=0.125$ and $1.375$ . . . . .	164
7.17	OTJ vorticity contours at $x/D=0.125$ and $2.625$ . . . . .	165
7.18	Comparison of streamline features and vorticity contours in the SDTJ flow. . .	167
7.19	Comparison of streamline features and vorticity contours in the OTJ flow. . . .	168
7.20	Diagram showing equivalent vorticity concentration and the Lamb-Oseen vortex. 169	
7.21	Vorticity and tangential-velocity distributions of the Lamb-Oseen vortex. . . . .	170
7.22	Bias error in vorticity calculation. . . . .	171
8.1	Conditionally-sampled SDTJ flow at cross-sections $x/D=0.125$ and $0.625$ . . .	175
8.2	Conditionally-sampled SDTJ flow at cross-sections $x/D=1.375$ and $2.250$ . . .	176
8.3	Conditionally-sampled OTJ flow at cross-sections $x/D=0.125$ and $0.625$ . . . .	177
8.4	Conditionally-sampled OTJ flow at cross-sections $x/D=1.375$ and $2.625$ . . . .	178
8.5	Path of the SDTJ/OTJ constructed from contours of r.m.s. velocity fluctuations. 180	
8.6	Streamlines in ensemble-averaged cross-sections of the SDTJ flow. . . . .	181
8.7	Streamlines in ensemble-averaged cross-sections of the OTJ flow. . . . .	181
8.8	Diagram illustrating the process of subdividing PIV data into smaller batches. .	182
8.9	Small-batch-size streamlines in cross-sections of the SDTJ flow. . . . .	183
8.10	Small-batch-size streamlines in cross-sections of the OTJ flow. . . . .	184
8.11	Apparent location of SDTJ and OTJ reattachment points. . . . .	187
8.12	A replot of Figure 8.7 accounting for detection-time lag. . . . .	189
8.13	SDTJ vorticity distribution at cross-sections $x/D=0.125, 0.375$ and $0.875$ . . .	190
8.14	SDTJ vorticity distribution at cross-sections $x/D=1.375, 1.750$ and $2.250$ . . .	191
8.15	OTJ vorticity distribution at cross-sections $x/D=0.125, 0.375$ and $0.875$ . . . .	192
8.16	OTJ vorticity distribution at cross-sections $x/D=1.375, 1.750$ and $2.625$ . . . .	193
8.17	SDTJ vortex skeleton constructed from PIV streamlines. . . . .	195
8.18	OTJ vortex skeleton constructed from PIV streamlines. . . . .	196
8.19	Ensemble-average circulation of the SDTJ and OTJ flows. . . . .	198
8.20	Diagram showing possible variation of the SDTJ/OTJ vortex cores with time. .	199
8.21	Effect of instantaneous vortex structure on the distribution of circulation. . . . .	200
8.22	Schematic reconstruction of the SDTJ and OTJ flows. . . . .	202
8.23	Revision of SDTJ flow topology from Figure 5.16. . . . .	203
8.24	The OTJ flow topology. . . . .	203
8.25	The Guo et al. [2001] simulation of oscillating flow through an abrupt expansion. 205	
8.26	Flow field in longitudinal section of the OTJ nozzle. . . . .	207

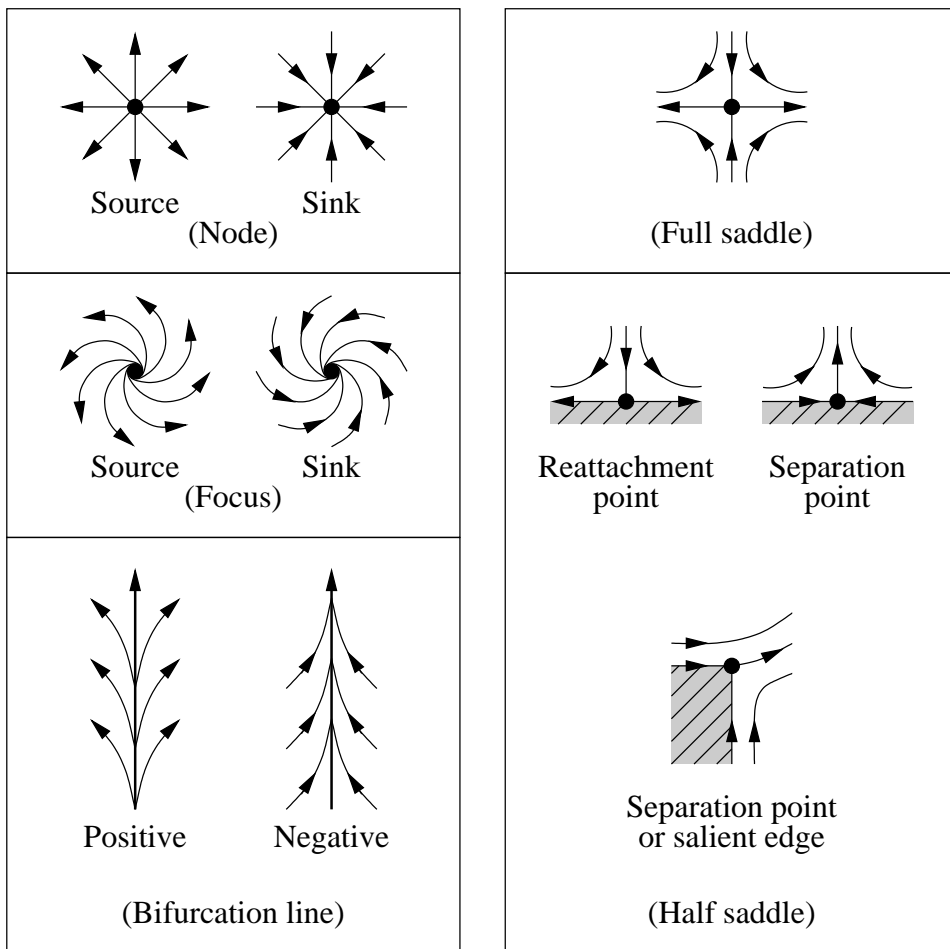
8.27	Flow field from Figure 8.26 readjusted to fit the Wong et al. [2003] data. . . . .	207
9.1	The OTJ nozzle and its flow field. . . . .	211
9.2	Structure of the SDTJ flow. . . . .	213
9.3	The unwrapped surface-flow topology in the OTJ nozzle. . . . .	214
9.4	Schematic reconstruction of the vortex skeletons of the SDTJ flow and OTJ flow.	215
A.1	Flow from a lossless contraction nozzle. . . . .	227
B.1	Circuit diagram of directional event detector. . . . .	230
C.1	The OTJ-nozzle coordinate system, dimensions and control-volume definitions.	232
D.1	Cross-section of the (internal) SDTJ flow at streamwise location $x/D=0.125$ . .	239
D.2	Cross-section of the (internal) SDTJ flow at streamwise location $x/D=0.375$ . .	240
D.3	Cross-section of the (internal) SDTJ flow at streamwise location $x/D=0.625$ . .	241
D.4	Cross-section of the (internal) SDTJ flow at streamwise location $x/D=0.875$ . .	242
D.5	Cross-section of the (external) SDTJ flow at streamwise location $x/D=1.375$ . .	243
D.6	Cross-section of the (external) SDTJ flow at streamwise location $x/D=1.750$ . .	244
D.7	Cross-section of the (external) SDTJ flow at streamwise location $x/D=2.250$ . .	245
D.8	Cross-section of the (internal) OTJ flow at streamwise location $x/D=0.125$ . .	246
D.9	Cross-section of the (internal) OTJ flow at streamwise location $x/D=0.375$ . .	247
D.10	Cross-section of the (internal) OTJ flow at streamwise location $x/D=0.625$ . .	248
D.11	Cross-section of the (internal) OTJ flow at streamwise location $x/D=0.875$ . .	249
D.12	Cross-section of the (internal) OTJ flow at streamwise location $x/D=1.375$ . .	250
D.13	Cross-section of the (internal) OTJ flow at streamwise location $x/D=1.750$ . .	251
D.14	Cross-section of the (external) OTJ flow at streamwise location $x/D=2.625$ . .	252

# List of Tables

1.1	Studies of oscillating-jet flow. . . . .	3
1.2	Some chemical reactions of nitrogen oxides. . . . .	6
1.3	Chemical reactions in a cement kiln [Spang, III, 1972]. . . . .	11
2.1	Summary of topics on FPJ flow. . . . .	21
4.1	Characteristics of the oscillating-jet flames. . . . .	74
6.1	Accumulated radial force on the OTJ flow and SDTJ flow in the chamber. . . . .	128
6.2	Review of FPJ Strouhal-number measurements. . . . .	134
7.1	Parameters affecting velocity and spatial resolution of PIV measurements. . . . .	157
7.2	Dynamic ranges of velocity and spatial resolution. . . . .	157
7.3	Accuracy of velocity measurements. . . . .	161
7.4	Accuracy of vorticity measurements. . . . .	171



Nozzle components and geometric parameters.



Critical points and bifurcations.

# Notation

## *Geometric parameters and coordinate system*

$D$	chamber diameter
$D_0$	inlet-pipe diameter
$d_1, d_{e1}$	inlet-orifice (equivalent) diameter
$d_2$	exit-lip diameter
$L$	chamber length
$x, y, z$	streamwise, horizontal and vertical scales/directions

## *Jet-flow parameters*

$f_p$	precession/oscillation frequency
$P$	pressure
$P_0$	inlet-pipe pressure
$P_\infty$	ambient pressure
$Q$	supply flow rate through the nozzle
$q_1$	dynamic pressure of bulk flow through the inlet orifice, $q_1 = \frac{1}{2}\rho U_1^2$
$t$	time
$U_0$	bulk flow velocity in the inlet pipe, $U_0 = Q / (\frac{1}{4}\pi D_0^2)$
$U_1$	bulk flow velocity at the inlet orifice, $U_1 = Q / (\frac{1}{4}\pi d_{e1}^2)$
$U_{cl}$	nozzle-centreline flow speed

## *Coefficients and dimensionless groups*

$C_d$	discharge coefficient of the inlet-orifice flow, $C_d = \sqrt{\frac{1}{K-1} [(D_0/d_{e1})^4 - 1]}$
$C_p$	pressure coefficient, $C_p = P/q_1$
$K$	loss coefficient of supply flow through the nozzle, $K-1 = (P_0 - P_\infty) / (\frac{1}{2}\rho U_0^2)$
$Re_0$	Reynolds number of the inlet-pipe flow, $Re_0 = D_0 U_0 / \nu$
$Re_1$	Reynolds number of the inlet-orifice flow, $Re_1 = d_{e1} U_1 / \nu$
$St_1$	Strouhal number of the inlet-orifice flow, $St_1 = f_p d_{e1} / U_1$

*Flow-topology symbols*

$F$	focus/vortex
$N$	node
$NB$	negative-bifurcation line
$PB$	positive-bifurcation line
$S$	saddle point

*Greek Symbols*

$\Lambda$	decay rate of jet-flow speed along the nozzle centreline
$\nu$	kinematic viscosity of working fluid
$\omega$	vorticity
$\Phi$	azimuthal angle
$\pi$	circumference-to-diameter ratio of a circle
$\rho$	density of working fluid
$\Theta$	jet-spreading angle

*Other symbols*

$\mathbf{f}(\dots)$	a function of a parameter
$\langle \dots \rangle$	ensemble average (or average of conditionally-sampled data)

*Abbreviations*

FPJ	fluidic precessing jet (as shown below)
OTJ	oscillating triangular jet
SDTJ	stationary deflected triangular jet

## NOTE:

This figure is included on page xxii of the print copy of the thesis held in the University of Adelaide Library.

Air-bubble flow visualisation in the FPJ nozzle (from Nathan et al. [1998]).  
Inlet orifice and exit lip are at ① and ②, respectively. Greyscales are inverted.